ORIGINAL PAPER

Structure and spacing of cellulose microfibrils in woody cell walls of dicots

**Lynne H. Thomas · V. Trevor Forsyth ·
Anne Martel · Isabelle Grillo ·
Clemens M. Altaner · Michael C. Jarvis**

Abstract The structure of cellulose microfibrils in situ in wood from the dicotyledonous (hardwood) species cherry and birch, and the vascular tissue from sunflower stems, was examined by wide-angle X-ray and neutron scattering (WAXS and WANS) and small-angle neutron scattering (SANS). Deuteration of accessible cellulose chains followed by WANS showed that these chains were packed at similar spacings to crystalline cellulose, consistent with their inclusion in the microfibril dimensions and with a location at the surface of the microfibrils. Using the Scherrer equation and correcting for considerable lateral disorder, the microfibril dimensions of cherry, birch and sunflower microfibrils perpendicular to the [200] crystal plane were estimated as 3.0, 3.4 and 3.3 nm respectively. The lateral dimensions in other directions were more difficult to correct for disorder but appeared to be 3 nm or less. However for cherry and sunflower, the microfibril spacing estimated by SANS was about 4 nm and was insensitive to the presence of moisture. If the microfibril width was 3 nm as estimated by WAXS, the SANS spacing suggests that a non-cellulosic polymer segment might in places separate the aggregated cellulose microfibrils.

Keywords WAXS · WANS · SANS · Crystallinity · Scherrer · Wood

L. H. Thomas
Department of Chemistry, University of Bath, Claverton Down, Bath BA2 7AY, UK

V. T. Forsyth · A. Martel · I. Grillo
Institut Laue-Langevin, 38042 Grenoble Cedex 9, France

V. T. Forsyth
EPSAM/ISTM, Keele University, Staffordshire ST5 5BG, UK

C. M. Altaner
New Zealand School of Forestry, University of Canterbury, Christchurch 4180, New Zealand

M. C. Jarvis (✉)
School of Chemistry, Glasgow University, Glasgow G12 8QQ, UK
e-mail: mikej@chem.gla.ac.uk

Abbreviations
NMR	Nuclear magnetic resonance
WAXS	Wide angle X-ray scattering
WANS	Wide angle neutron scattering
SANS	Small angle neutron scattering

Introduction

Cellulose microfibrils from higher plants are long, partially crystalline, fibrous units a few nanometers in diameter. Certain algal species synthesise thicker and more crystalline microfibrils comprising several hundred parallel cellulose chains packed together in one of

two well-ordered lattices, cellulose Iα and cellulose Iβ. (Nishiyama et al. 2002; Nishiyama et al. 2003).

The Iα and Iβ forms were first distinguished by solid-state nuclear magnetic resonance (NMR) spectroscopy (Atalla and Vanderhart 1984) and their structures were established by X-ray and neutron diffraction studies on algal and tunicate celluloses (Nishiyama et al. 2002, 2003). In NMR spectra from the thinner and more disordered microfibrils of softwood (gymnosperm) cellulose, it is possible to distinguish structural features similar to the Iα and Iβ forms (Newman 1999), but only in 30–40 % of the cellulose present, because the crystallinity is so low (Newman 2004; Thygesen et al. 2005).

The high level of disorder presents a challenge to structure determination by any method, but evidence has been presented for spruce microfibrils approximately 3 nm in diameter (Andersson et al. 2003; Fernandes et al. 2011) allowing space for approximately 20 chains. Models for 18- and 24-chain spruce microfibrils have been proposed on the basis of NMR, SANS and disorder-corrected WAXS (Scherrer) measurements (Fernandes et al. 2011). Similar, but still more disordered structures have been suggested for microfibrils of cellulose in the primary (growing) cell walls of higher plants (Thomas et al. 2013b) for which it has been shown that the WAXS patterns can be simulated by 18-chain models with some of the microfibrils coalescing, at least for short lengths, through the relatively hydrophobic [200] crystallographic plane (Newman et al. 2013). Such models would be consistent with the available evidence on spruce microfibrils (Fernandes et al. 2011).

In addition to the proposed short-range coalescence of softwood microfibrils, where the crystal lattice is continuous across the interface, they are known to be aggregated into bundles about 10–20 nm across without continuity of crystalline structure between individual microfibrils (Fahlen and Salmen 2005; Donaldson 2007; Fernandes et al. 2011). The majority of the hemicellulose and lignin content of softwoods is likely to be situated outside these microfibril bundles (Fahlen and Salmen 2005; Xu et al. 2007; Fernandes et al. 2011; Terashima et al. 2009).

For woody dicots (hardwoods) the structure of the microfibrils and their degree of aggregation is uncertain although there is evidence that aggregation does occur in poplar wood (Donaldson 2007). Here we present X-ray and neutron scattering data on two typical hardwood species, cherry and birch, together with woody tissue from sunflower stems.

Materials and methods

Materials

Japanese Cherry (*Prunus serrulata*) and downy birch (*Betula pubescens*) wood were obtained from the sapwood (outer) region of trees aged 22 and 37 years respectively. Sunflowers (*Helianthus annuus*) were grown to maturity, reaching a height of 2.5 m, and the vascular ring from the stem base was excised and stripped of parenchyma tissue with a scalpel.

Small-angle neutron scattering (SANS)

Small-angle neutron scattering analysis was conducted on beamline D33 at the Institut Laue-Langevin (ILL), Grenoble. The neutron beam had a wavelength of $\lambda = 3.5$ Å (with $\Delta\lambda = 10$ %) Å and a 2.8 m long rectangular collimation was used. Sample-to-detector distance was 2 m. The q range covered in this experiment extended from 0.4 to 2.8 nm^{-1}. Samples 2 mm in thickness were adjusted to the desired moisture content by saturating with H_2O, D_2O or 35:65 D_2O:H_2O then equilibrating with phosphorus pentoxide to dry to a predetermined weight, encapsulating in aluminium foil and allowing at least 1 h for internal equilibration of moisture. An empty foil container was used as background.

The contrast matching solvent, 35:65 D_2O:H_2O was chosen based on a neutron scattering length density of 194 fm/nm^3, calculated from the atomic scattering lengths (Sears, 1992), the elemental composition and the volume of the cellulose Iβ unit cell (Nishiyama et al., 2002). For cellulose chains at accessible microfibril faces it was assumed that on average 1.5 hydroxyls were exposed per monomer residue, increasing the calculated scattering length density to 291 fm/nm^3 when exchanged against pure D_2O or 228 fm/nm^3 in 35:65 D_2O:H_2O. For hemicellulosic xylan and syringyl lignin the scattering length density was derived similarly but the monomer volume was calculated as Molecular mass/(bulk density × Avogadro number). The bulk density in situ depends on conformation and packing and is the main source of uncertainty: a value of 1.3 g/cm^3 for both lignin and

hemicelluloses in hydrated wood (Harrington 2002) was used, leading to scattering length densities of 170 fm/nm^3 for lignin and 200 fm/nm^3 for xylan in equilibrium with 35:65 D_2O:H_2O, assuming all the xylan hydroxyls are accessible.

Wide-angle X-ray scattering (WAXS)

X-ray diffraction patterns were obtained at ambient temperature using a Rigaku R-RAPID image plate diffractometer. A Mo Kα ($\lambda = 0.07071$ nm) source was used, with the beam collimated to a diameter of 0.5 mm. Scattering angles were expressed as $q = 4\pi\sin\theta/\lambda$ Samples were 1 or 2 mm thick in the direction parallel to the beam and their other dimensions exceeded the beam diameter. The diffraction patterns were collected in perpendicular transmission mode. Radial profiles of scattered intensity I as a function of q were integrated over azimuthal angles of 2° using the AreaMax software package (Rigaku/MSC, Tokyo). Background correction was carried out as described by Fernandes et al. (2011). Each tangential profile was fitted by a dual Gaussian function and the narrower of the two Gaussians was used to reconstruct the equatorial radial profile (Thomas et al. 2013a). Asymmetric peak functions were fitted to these equatorial profiles as described by Fernandes et al. (2011). It was assumed that a plot of peak width F against the square of the order of reflection r^2 is linear for the 200 and 400 reflections with, at the intercept, the Scherrer dimension (mean column length) L $= k\lambda/F\cos\theta$ using the Scherrer constant $k = 0.94$ as appropriate for a cylindrical crystallite.

Wide-angle neutron scattering (WANS)

Wood samples approximately 15 mm × 10 mm × 2 mm, or fragments of sunflower xylem packed into sheets of similar dimensions, were fully dried, adjusted in hydration/deuteration level and encapsulated in aluminium foil as described for SANS.

Wide angle neutron scattering analysis was conducted on beamline D19 at the Institut Laue-Langevin (ILL), Grenoble, France. Beamline D19 has a four-circle diffractometer with a cylindrical detector consisting of a 256 × 640 array of gas-filled cells giving an aperture 30° vertically × 120° horizontally. The neutron wavelength was 2.42 Å and the sample-to-detector distance, taken to the electrode plane in each

cell at the equator, was 756 mm. The response for each cell of the detector was calibrated using the isotropic incoherent neutron scattering from a vanadium rod, and blank-corrected using an empty aluminium foil container.

The absorption coefficient of each sample along the beam axis was calculated from absorption coefficients based on the elemental composition. Absorption factors at all angles within the aperture of the detector were then calculated using in-house software based on the integrated path length through the sample, which was assumed to have cuboidal geometry and was wider than the neutron beam. The fibre axis was tilted such that the full widths of the 001, 002, 003 and 004 reflections were collected. In-house software was then used to remap the data into reciprocal space and to join together the component images of the diffraction pattern. The combined images were exported into Fit2D, where radial intensity profiles integrated over 10° in azimuth were calculated in the equatorial and meridional directions.

Results

Wide-angle X-ray scattering

The fibre diffraction (WAXS) patterns from woody cell walls of all three dicotyledonous species, birch, cherry and sunflower, were well-oriented and dominated by reflections from cellulose. In each case the azimuthal intensity distribution of the 200 (equatorial) reflection, representing the intersheet spacing of the cellulose lattice, could be separated into three components. A minor isotropic component, presumably derived at least in part from primary cell walls, was removed with the background scattering. A broad component was modelled as a Gaussian distribution with s = 16° leaving a narrow component of comparable intensity, also modelled as a Gaussian distribution with s = 6.3° for birch, 7.5° for cherry and 5.9° for sunflower cellulose. These azimuthal distributions are comparable with distributions observed for mature, old-growth Sitka spruce wood (Fernandes et al. 2011) and imply well-oriented cellulose microfibrils.

Radial intensity distributions for the equatorial reflections are shown in Fig. 1. The [200] *d*-spacings of 0.394 and 0.396 nm observed for birch and cherry
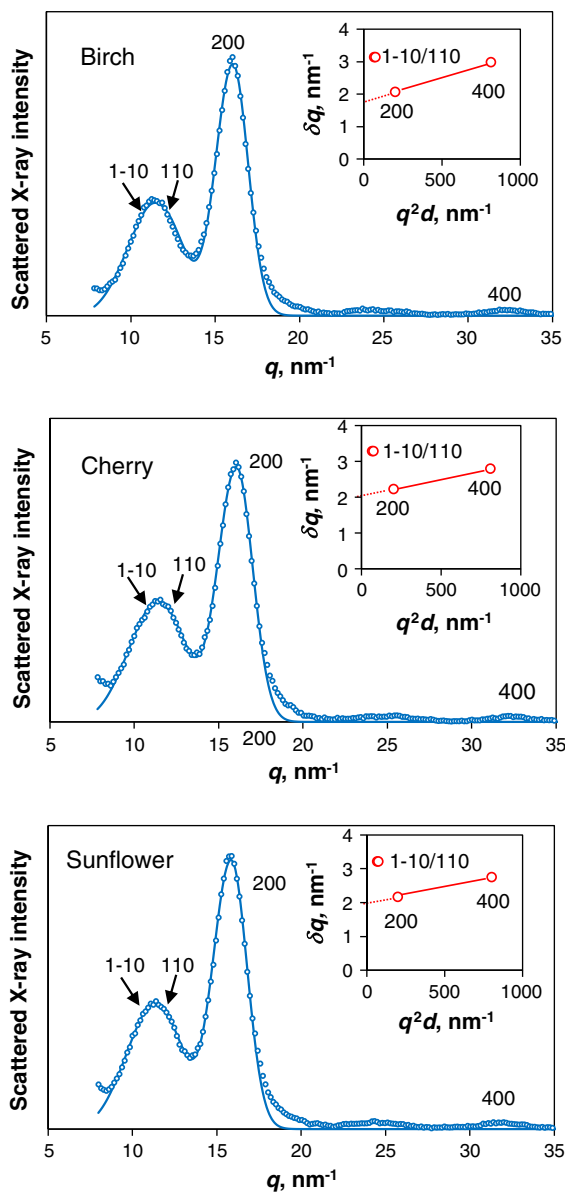
Fig. 1 Wide-angle X-ray scattering. Radial equatorial profiles of scattering intensity. The vertical scale is in arbitrary units. On the horizontal axis, the scattering angle is expressed as $q = 4\pi \sin\theta/\lambda$ The 200 reflection is at $q = 16$ nm^{-1}, the 400 reflection is at $q = 32$ nm^{-1} and the 1-10 and 110 reflections overlap at $q = 10$-12 nm^{-1}. The observed scattering intensity profile (*open circles*) was fitted with summed, asymmetrically adjusted Gaussian functions for these reflections. The same asymmetry function was used for all reflections, the widths of the 1–10 and 110 reflections were assumed to be the same and their spacing was calculated from a monoclinic angle of 97°. *Inset* plot of radial broadening δq against q^2d, where d is the lattice spacing concerned. The column length (microfibril diameter) perpendicular to the [200] lattice planes is derived from the intercept of the *line* joining the 200 and 400 reflections, but the 1–10 and 110 reflections lie above this *line*

cellulose respectively were close to those observed for coniferous wood but the [200] *d*-spacing of 0.398 nm observed for sunflower cellulose was closer to that expected for primary-wall celluloses. The 1–10 and 110 reflections were strongly overlapped in all three samples as normally found for celluloses of relatively low crystallinity (Thomas et al. 2013b).

The radial broadening of these equatorial reflections is an indication of the extent of disorder within the cellulose lattice, and also of the small lateral dimensions of the microfibrils. The influences of dimensions and disorder are difficult to separate, but this can be done by progressively removing the broadening contributions of disorder of different kinds, correcting for instrumental broadening and then using the Scherrer equation to match the remaining broadening to predicted lateral dimensions (Fernandes et al. 2011; Thomas et al. 2013a, b). A more fundamental approach is to predict the radial intensity profile by first-principles calculation from an ensemble of structures simulating the disorder assumed to be present (Newman 2008; Newman et al. 2013). These two approaches give comparable results although the first-principles approach shows that in structures containing only a few lattice planes, the Scherrer equation becomes an approximation (Newman 2008).

By first modelling out asymmetric broadening and then using a plot of the residual broadening δq against q^2d to separate the effects of 'paracrystalline' disorder and small Scherrer dimensions (Fernandes et al. 2011; Thomas et al. 2013a), it was evident (Fig. 1) that the microfibril dimension perpendicular to the [200] lattice plane was similar to that of Sitka spruce. The broadening of the 1–10 and 110 reflections was greater than for the 200 and 400 reflections, as can be seen in the δq against q^2d plots where those points lie above the line joining the 200 and 400 reflections. This feature was also evident in the diffraction data for spruce and celery cellulose (Fernandes et al. 2011; Thomas et al. 2013b), but was more pronounced in the present experiments. In principle it indicates either more disorder or smaller dimensions perpendicular to the [1–10] and [110] lattice planes than perpendicular to the [200] lattice plane, but practical problems reduce the certainty of this deduction: the estimated broadening of the 1–10 and 110 reflections is very sensitive to the value assumed for the monoclinic angle, and the calculated Scherrer dimensions, each of which represents a weighted-mean column length

perpendicular to the lattice plane in question, are sensitive to the shape assumed for the microfibril. Newman et al. (2013), matching predicted diffraction data mainly against the observed 200 reflection, suggested that a range of shapes were present but that the dimension perpendicular to the [200] lattice plane was increased by occasional 'stacking' or 'twinning' of microfibrils in this direction. The δq vs $q^2 d$ plots in Fig. 1 are consistent with this interpretation, suggesting mean microfibril dimensions (column lengths) of 3.4, 3.0 and 3.3 nm in this direction for microfibrils of birch, cherry and sunflower cellulose respectively.

Wide-angle neutron scattering

Neutron diffraction (WANS) patterns from wood cellulose are in general similar to X-ray diffraction patterns except that the intensity of the reflections is strongly affected when accessible protons are replaced by deuterium. Hydroxyl protons in the interior of the cellulose lattice are inaccessible to deuteration. Hydroxyl protons exposed on the microfibril surface are accessible provided that they are not located at a tight, hydrogen-bonded interface with a neighbouring microfibril (Thomas et al., 2013b). In principle hydroxyl groups in disordered regions within the microfibril might also be expected to be accessible, but this would require significant expansion of the lattice to permit access for D_2O and the change in d-spacing should then be readily detectable. WANS therefore permits any structural differences between surface or disordered domains and crystalline domains to be identified.

Figure 2 shows that there were substantial differences between the equatorial scattering profiles of the deuterated and non-deuterated samples from all three species. The (D-H) subtraction profiles (Fig. 2) for all three species were positive at the q value of the 200 reflection and negative at the q value of the 110 reflection. In cellulose Iβ, complete deuteration (which requires more extreme conditions) slightly increases the relative intensity of the 200 reflection and greatly decreases the relative intensity of the 1-10 reflection (Nishiyama et al. 2002) due to the large difference in coherent scattering length between H and D and the consequent effect on the structure factor for each reflection (Thomas et al. 2013b). Within the limitations of the signal:noise ratio and q resolution,
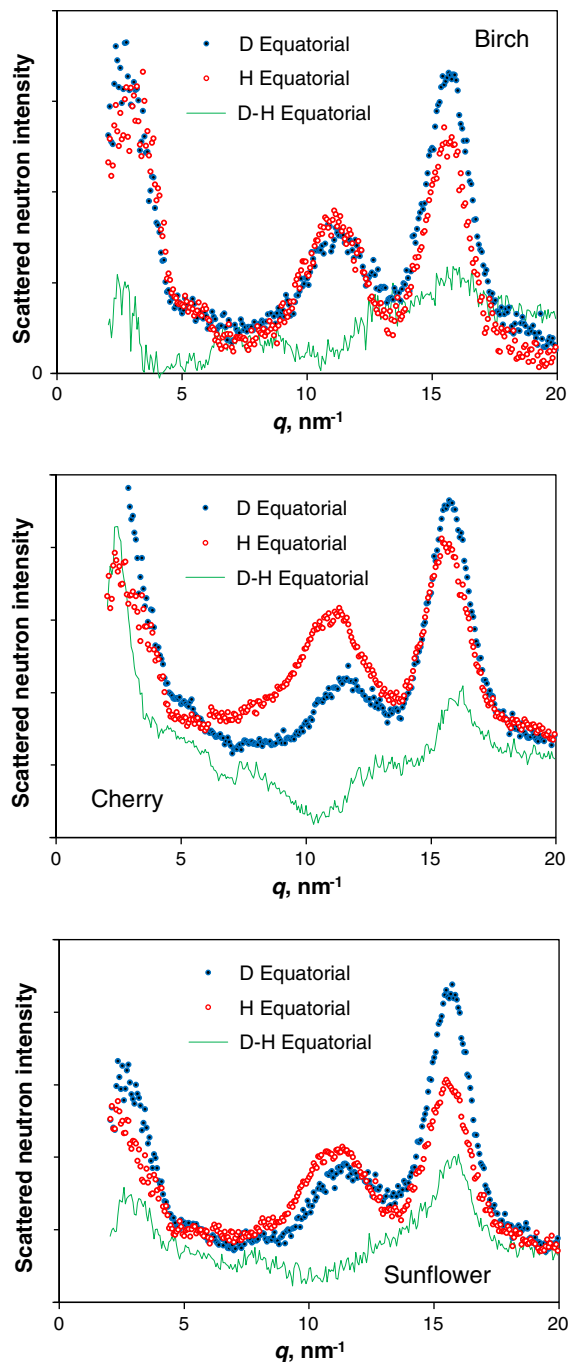
Fig. 2 Radial equatorial profiles of wide-angle neutron scattering intensity. The vertical scale is in arbitrary units. Samples were equilibrated in the vapour phase with either H_2O or D_2O, hydrating or deuterating accessible hydroxyl groups. The difference profile (D-H) identifies reflections from accessible chains

these positive and negative peaks in the (D-H) subtraction profile were similar in q value to the corresponding reflections in the H form (and in the WAXS pattern), implying that the hydroxyl groups accessible to deuteration were located on chains at similar d-spacings to the crystalline cellulose fraction. Deuteration of disordered domains within the microfibril would require wider spacings for D_2O access, leading to reduced q. No reduction in q was observed. If anything for the 200 reflection q appeared to increase, but the change was too small to be meaningful. The implication is that the deuteration-accessible chains were not in the microfibril interior but at the surface, and were packed at spacings corresponding to an extension of the crystalline lattice forming the interior. It is not necessary that the surface chains should share the conformation and hydrogen-bonding pattern of the interior chains, and in conifer celluloses there are indeed conformational differences (Fernandes et al. 2011).

Small-angle neutron scattering (SANS)

Semi-regular aggregation of well-oriented cellulose microfibrils in primary cell walls permits small-angle Bragg scattering of X-rays and neutrons, allowing the centre-to-centre spacing of the microfibrils to be calculated: their spacing increases on hydration (Kennedy et al. 2007; Thomas et al. 2013b). Hydrated or deuterated spruce wood showed similar Bragg scattering but only with neutrons (Fernandes et al. 2011). The scattered neutron intensity and the microfibril spacing diminished with drying until fully dried, but surface-deuterated, spruce microfibrils showed a very weak Bragg peak at 3 nm spacing, considered to represent the centre-to-centre distance of microfibrils in contact, which is equivalent to the microfibril diameter (Fernandes et al. 2011).

Small-angle neutron scattering patterns from deuterated birch, cherry and sunflower cell walls showed weaker Bragg scattering than from spruce wood but the Bragg intensity was affected very little by drying (Fig. 3). The microfibril spacing also was hardly affected by drying and remained around 4 nm even when the dicotyledonous samples were fully dried. A similar SANS d-spacing for microfibrils in aspen *(Populus tremuloides)*, also a dicot, has been reported (Nishiyama et al. 2014). For birch and cherry wood the small-angle Bragg peak disappeared on

equilibration with moisture at the neutron scattering contrast match point for cellulose (35 % D_2O/65 % H_2O). For sunflower cell walls under these conditions, unusually, a very weak small-angle Bragg peak remained at higher q corresponding to a d-spacing of approximately 3.0 nm. The origin of this feature is uncertain but it would appear to correspond to partially surface-deuterated microfibrils in direct contact with one another.

It should be noted that only domains in which neutron scattering contrast is generated by deuteration, or by large differences in local density, give rise to the observed small-angle Bragg scattering. If aggregation is irregular then gaps between microfibrils that are wide enough to admit D_2O molecules are the most likely to be deuterated and make the largest contribution to the neutron scattering intensity.

Discussion

Sunflowers are not trees, but in view of the large bending stresses that the vascular ring must withstand in slender sunflower stems, the close similarity in sunflower cellulose structure to wood from the two hardwood species examined was of interest. The microfibril angle (deviation of microfibril orientation from the stem axis) was, remarkably, less in the case of sunflower stems than for most trees, suggesting possibilities for the exploitation of sunflower straw as a source of high-performance cellulosic fibre. The only evident abnormality was a slightly increased intersheet spacing, a feature commonly found in primary-wall celluloses (Thomas et al. 2013b).

The broadening of the 200 reflection in the WAXS patterns from the cherry and sunflower samples was similar to that observed in spruce wood (Fernandes et al. 2011) and celery collenchyma cellulose (Thomas et al. 2013b), after corrections had been made for the considerable amount of disorder identifiable. For cherry and sunflower microfibrils, therefore, a diameter ('height') of 3.0–3.3 nm perpendicular to the sheets of chains seems likely.

The WANS data showed that the dimensions estimated by wide-angle scattering are effectively the dimensions of the whole microfibril, not just the crystalline core, because its d-spacings are shared by the deuteration-accessible surface chains. This observation also showed that the chains accessible to
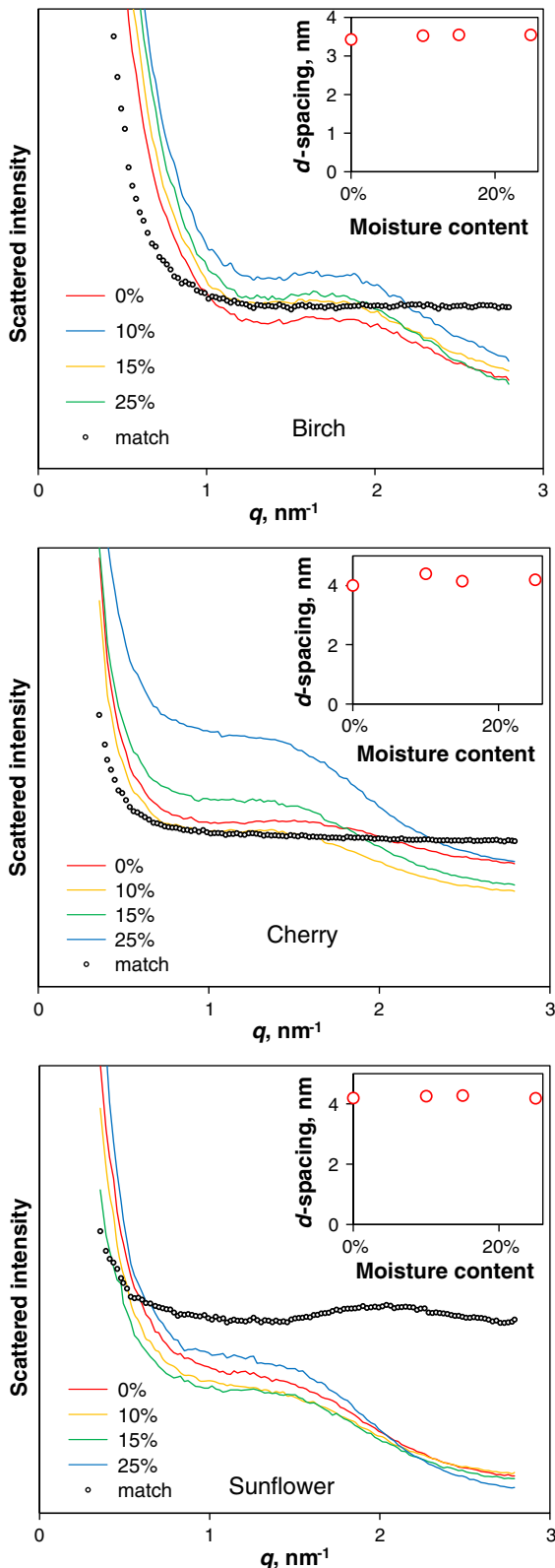
◀**Fig. 3** Radial equatorial profiles of small-angle neutron scattering intensity. The vertical scale is in arbitrary units. Samples were equilibrated to varying moisture contents with D_2O. Each scattering curve was separated into a dual-exponential background and a broad Bragg peak derived from coherent scattering from loosely arrayed microfibrils. *Inset* Variation in the calculated *d*-spacing of the small-angle Bragg peak (microfibril centre-to-centre spacing) after subtraction of the dual-exponential non-coherent scattering background

deuteration were predominantly located at the microfibril surfaces, and their intersheet spacing was too narrow to be consistent with the presence of loosely packed disordered domains in the centre of the microfibrils. The relatively large broadening perpendicular to the [1–10] and [110] crystal planes, although difficult to quantify given the influence of the monoclinic angle, tends to imply either that there was more disorder in that direction than in spruce or primary-wall microfibrils, or that the mean dimension across the sheets of chains ('width'), corresponding approximately to three chains side-by-side, was smaller than the 3 nm estimated for these other celluloses.

The SANS experiments gave results quite different from those obtained for spruce wood (Fernandes et al. 2011) and primary-wall cellulose (Thomas et al. 2013b). Because SANS contrast depends on deuterium-rich domains between microfibrils, the spacing recorded is likely to be across hydrophilic interfaces, not across the hydrophobic junction of the [200] faces. For sunflower and cherry wood the microfibril spacings calculated from the position of the SANS Bragg peak were about 4 nm, considerably greater than the microfibril width estimated by WAXS, and did not change on hydration.

Considerable experimental difficulties attended the estimation of microfibril widths using either small-angle or wide-angle scattering, but the discrepancy between the width estimates was large enough to invite potential explanations. One explanation is that for most of their length, microfibrils about 3 nm wide were too tightly aggregated to allow deuterium exchange, but that the SANS contrast came from short regions where a non-cellulosic polymer or bound water (Nishiyama et al. 2014) was interposed between two aggregated microfibrils, allowing access for D_2O and deuteration of any hydroxyls on the interstitial polymer together with those on the adjacent

cellulose surfaces. The contrast matching experiment, which eliminated the Bragg peak corresponding to the 4 nm SANS *d*-spacing, would be easier to reconcile with an inserted xylan segment rather than a segment of a lignin chain because xylan, when equilibrated with the contrast matching solvent and bound to a cellulose surface, has a scattering length density closer to that of cellulose. The 4 nm *d*-spacing would provide room for a xylan chain segment fitted between the hydrophilic faces of two 3 nm microfibrils, with the xylan ring plane in a different orientation so that it would not contribute to the width of the cellulose lattice. A chain segment of syringyl lignin would be more likely to bind to the hydrophobic faces of the microfibrils. The faint SANS peak that survived contrast matching in sunflower cell walls, corresponding to a 3 nm *d*-spacing, may reflect direct packing of partially surface-deuterated 3 nm sunflower microfibrils along their hydrophilic faces as in celery primary-wall cellulose (Thomas et al. 2013b).

An alternative explanation is that the microfibrils were about 4 nm wide, equivalent to the SANS spacing and wider than was observed for primary-wall and spruce cellulose (Fernandes et al. 2011; Thomas et al. 2013b). That could be the case if very high levels of disorder at the hydrophilic faces of the microfibril prevented its increased width from leading to reduced broadening of the 1–10 and 110 reflections in WAXS and WANS. It should be noted that disorder in these directions cannot be measured directly from the diffraction data, and was instead approximated as being equal to disorder in the [200] direction. However disorder, in the most likely form of loose chain packing at the edges of the microfibril, would be expected to lead to increased [1–10] and [110] *d*-spacings in WANS after deuteration. This was not observed.

The uncertainty as to the microfibril 'width' across the sheets of chains makes it difficult to calculate the cross-sectional area and hence the number of chains in a hardwood microfibril. If the width is set equal to the SANS spacing, a 3.2 × 4 nm microfibril would have room for 30-36 chains, depending on its shape. It would then be necessary to propose that microfibrils in secondary cell walls of dicots are synthesised (Slab-augh et al. 2013) in a way that incorporates more chains than in primary cell walls or in gymnosperm wood. If the microfibril width is only about 3 nm, on the other hand, the cross section would be similar to

these other celluloses, consistent with the similarity in their WAXS patterns. The WAXS pattern from mung bean primary-wall cellulose could be matched best by an ensemble of irregular 18-chain microfibril models, with some degree of stacking in pairs joined through the hydrophobic [200] faces (Newman et al. 2013) increasing the mean height to about 3 nm. An increased degree of stacking of this kind is a potential explanation of the smaller broadening of the 200 reflection from birch wood, which led to an estimated height of 3.4 nm.

This 'stacking', with coalescence of the lattices of adjacent microfibrils, must be distinguished from aggregation where the lattices remain distinct. Aggregation of microfibrils into larger bundles (Donaldson 2007) is not as well documented in dicotyledonous species as in softwoods. These experiments show that in woody cell walls of dicotyledons, microfibrils are indeed aggregated but not in quite the same way: there appeared to be tighter microfibril-to-microfibril contact than in softwoods, and less access for water except where hemicelluloses were interposed. These findings have implications for the location of water binding within the structure of hydrated wood, and may contribute to explanations for differences between softwoods and hardwoods in the influence of moisture on mechanical performance, pulping and conversion to biofuel.

References

Andersson S, Serimaa R, Paakkari T, Saranpaa P, Pesonen E (2003) Crystallinity of wood and the size of cellulose crystallites in Norway spruce (*Picea abies*). J Wood Sci 49:531–537

Atalla RH, Vanderhart DL (1984) Native cellulose—a composite of 2 distinct crystalline forms. Science 223:283–285

Donaldson L (2007) Cellulose microfibril aggregates and their size variation with cell wall type. Wood Sci Technol 41:443–460

Fahlen J, Salmen L (2005) Pore and matrix distribution in the fiber wall revealed by atomic force microscopy and image analysis. Biomacromolecules 6:433–438

Fernandes AN, Thomas LH, Altaner CM, Callow P, Forsyth VT, Apperley DC, Kennedy CJ, Jarvis MC (2011) Nanostructure of cellulose microfibrils in spruce wood. Proc Natl Acad Sci USA 108:E1195–E1203

Harrington JJ (2002) Hierarchical modelling of softwood hygro-elastic properties. PhD thesis, University of Canterbury, Christchurch

Kennedy CJ, Cameron GJ, Sturcova A, Apperley DC, Altaner C, Wess TJ, Jarvis MC (2007) Microfibril diameter in celery collenchyma cellulose: X-ray scattering and NMR evidence. Cellulose 14:235–246

Newman RH (1999) Estimation of the relative proportions of cellulose I alpha and I beta in wood by carbon-13 NMR spectroscopy. Holzforschung 53:335–340

Newman RH (2004) Homogeneity in cellulose crystallinity between samples of *Pinus radiata* wood. Holzforschung 58:91–96

Newman RH (2008) Simulation of X-ray diffractograms relevant to the purported polymorphs cellulose IVI and IVII. Cellulose 15:769–778

Newman RH, Hill SJ, Harris PJ (2013) Wide-angle X-ray scattering and solid-state nuclear magnetic resonance data combined to test models for cellulose microfibrils in mung bean cell walls. Plant Physiol 163:1558–1567

Nishiyama Y, Langan P, Chanzy H (2002) Crystal structure and hydrogen-bonding system in cellulose 1 beta from synchrotron X-ray and neutron fiber diffraction. J Am Chem Soc 124:9074–9082

Nishiyama Y, Sugiyama J, Chanzy H, Langan P (2003) Crystal structure and hydrogen bonding system in cellulose 1(alpha), from synchrotron X-ray and neutron fiber diffraction. J Am Chem Soc 125:14300–14306

Nishiyama Y, Langan P, O'Neill H, Pingali SV, Harton S (2014) Structural coarsening of aspen wood by hydrothermal pretreatment monitored by small- and wide-angle scattering of X-rays and neutrons on oriented specimens. Cellulose 21:1015–1024

Sears VF (1992) Neutron scattering lengths and cross sections. Neutron News 3:26–37

Slabaugh E, Davis JK, Haigler CH, Yingling YG, Zimmer J (2013) Cellulose synthases: new insights from crystallography and modeling. Trends in Plant Science xx:1–8

Terashima N, Kitano K, Kojima M, Yoshida M, Yamamoto H, Westermark U (2009) Nanostructural assembly of cellulose, hemicellulose, and lignin in the middle layer of secondary wall of ginkgo tracheid. J Wood Sci 55:409–416

Thomas LH, Altaner CM, Jarvis MC (2013a) Identifying multiple forms of lateral disorder in cellulose fibres. J Appl Crystallogr 46:972–979

Thomas LH, Forsyth VT, Sturcova A, Kennedy CJ, May RP, Altaner CM, Apperley DC, Wess TJ, Jarvis MC (2013b) Structure of cellulose microfibrils in primary cell walls from collenchyma. Plant Physiol 161:465–476

Thygesen A, Oddershede J, Lilholt H, Thomsen AB, Stahl K (2005) On the determination of crystallinity and cellulose content in plant fibres. Cellulose 12:563–576

Xu P, Donaldson LA, Gergely ZR, Staehelin LA (2007) Dual-axis electron tomography: a new approach for investigating the spatial organization of wood cellulose microfibrils. Wood Sci Technol 41:101–116